Electronic Supplementary Material (ESI) for Physical Chemistry Chemical Physics.
This journal is © the Owner Societies 2023

Supplementary material to:

Subtle hydrogen bond preference and dual Franck-Condon activity – the interesting pairing of 2-naphthol with anisole

Arman Nejad,[a*] Ariel Pérez-Mellor,[b] Manuel Lange,[a] Ivan Alata,[b]
Anne Zehnacker[b] and Martin A. Suhm,[a]

[a] *Institute of Physical Chemistry, Georg-August University of Göttingen, Tammannstraße 6, 37077 Göttingen, Germany*
[b] *Institut des Sciences Moléculaires d'Orsay (ISMO), CNRS, Université Paris-Saclay, 91405 Orsay, France*
[*] *E-mail: anejad@gwdg.de*

Contents

S1 Experimental background information

An extended view of the FTIR spectra (Fig. 3, main text) is given in Fig. S1. The relative concentration of water (W) in the jet spectra is reflected in the relative intensity of its characteristic ro-vibrational OH stretching lines. The heating temperatures of 2-napththol (2N) and anisole (A) are included in the figure but are not reliable to assess their concentrations in the jet spectra. The CH stretching contours are much more useful and are, therefore, included. The characteristic regions to identify and compare the relative W/2N/A concentrations across the different spectra are highlighted in yellow.

The bare 2-naphthol spectra (grey) increase in concentration from bottom to top (i→iii). Trace (i) contains only negligible amounts of water, thus facilitating the assignment of bands E and F to 2-naphthol hydrates, *t*2NW and *c*2NW, respectively. Due to their different scaling with the 2-naphthol concentration, bands C and D correspond to different homocluster sizes. Based on the moderate 2-naphthol concentration in (i), we suggest that C corresponds to a homodimer.

Turning to the mixed spectra including anisole (black), we note that the overall signal enhancement from traces (a) and (b) to (c) and (d) illustrates the extended absorption path length in the new setup. The two upper traces in each pair (b and d) have overall higher 2-naphthol and anisole concentrations than the respective lower traces (a and c). Overall, there are three main new absorption regions that correspond to mixed 2-naphthol-anisole clusters, highlighted through two grey bars and the white space in-between. The main absorption feature in-between is observed even in the lowest-concentrated spectrum (a) whereas the features in the grey bars seem to be correlated. Because the signals in the right grey bar appearing in higher-concentration spectra (b and d) are likely due to trimeric or larger aggregates, this could also be the case in the left grey bar, close to 2-naphthol homocluster traces, where $c2NA_{\pi}$ would be expected at low intensity. The same applies to the even less abundant and visible $t2NA_{\pi}$, which is expected near 3600 cm^{-1}. Within the broad absorption around 3500 cm^{-1}, which roughly spans 60 cm^{-1}, there are several distinguishable peaks that we label G-J. Due to the presence of water impurities in the jet spectra, one might argue that G is not a new 2-naphthol-anisole band but actually a 2-naphthol hydrate signal (F). This is to a large extent the case for spectrum (a) but not (b) which displays only negligible amounts of water. By extension, this argument applies to spectra (c) and (d)

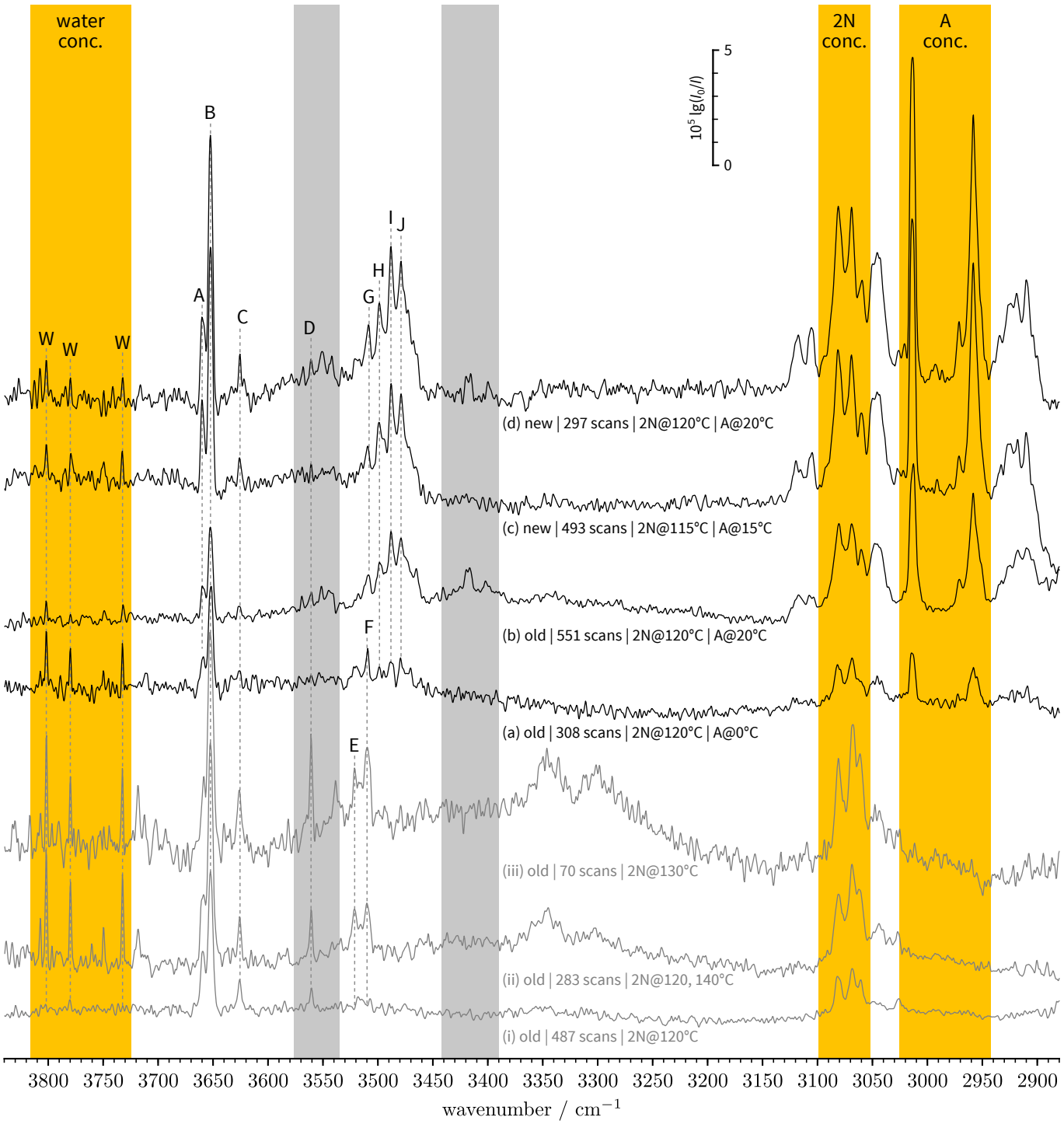

Fig. S1 FTIR decadic absorbance spectra (lg(I_0/I)) of bare 2-naphthol expansions (i-iii, grey) and 2-naphthol and anisole co-expansions (a-d, black) which have been recorded with the old (i-iii; a-b) and new setup (c-d). The band centres of A-J are compiled in Table 2 (main text). See text below for discussion.

where G, H, and I exhibit a similar intensity scaling ratio as in (b). Alternative assignments to anisole hydrates can similarly be ruled out. The mass- and conformer-selective IR-UV spectra (see Section 4.2, main text) confirm assignments of G-J to the two O-bound 1:1 2NA complexes (*c*2NA$_O$ and *t*2NA$_O$) and further reveal the excessive number of bands is due to a vibrational Franck-Condon-type progression of the ground state OH stretching vibration. The three bands G-H correspond to *c*2NA$_O$. While *t*2NA$_O$ is found to exhibit a similar progression, only J is fully resolved because the higher-wavenumber bands overlap with *c*2NA$_O$.

S2 Computational background information

Table S1 Comparison of relative energies ($\Delta E_{0,h}$), which are decomposed into purely electronic (ΔE_e) and harmonic zero-point vibrational ($\Delta\mathrm{ZPVE}_h$) contributions, and electronic dissociation energies (D'_e, Eq. 1 in main text) of the two computationally most stable 2NA conformers, $c2\mathrm{NA_O}$ and $c2\mathrm{NA}_\pi$. "ΔE_e(min)" compares the total $c2\mathrm{NA_O}$ PNO single-point energies across different reference geometries to identify which DFT geometry is closest to the 'true' coupled-cluster minimum (0) or farthest away (3.7). All quantities are in kJ mol^{-1}.

	B3LYP-D3(BJ)			B3LYP-D3$_{\mathrm{abc}}$(BJ)			PBE0-D3$_{\mathrm{abc}}$(BJ)			PBE0-D3(BJ)		
	S	TZ	QZ	S	TZ	QZ	S	TZ	QZ	S	TZ	QZ
DFT/def2-XVP												
$\Delta E_{0,h}^{\pi-\mathrm{O}}$	1.2	−0.7	−0.5	2.0	0.1	0.2	2.2	−0.7	−0.5	1.5	−1.0	−0.8
$\Delta\mathrm{ZPVE}_h^{\pi-\mathrm{O}}$	−1.5	−1.0	−1.1	−1.5	−0.8	−0.9	−1.7	−0.7	−0.9	−1.7	−0.7	−0.9
$\Delta E_e^{\pi-\mathrm{O}}$	2.8	0.3	0.6	3.5	0.9	1.2	3.9	0.0	0.4	3.2	−0.3	0.1
$D'_e[c2\mathrm{NA_O}]$	49.7	38.0	35.7	49.2	37.5	35.2	46.9	35.7	33.7	47.3	36.2	34.2
$D'_e[c2\mathrm{NA}_\pi]$	46.9	37.6	35.1	45.7	36.6	34.0	43.0	35.7	33.3	44.1	36.5	34.1
PNO-LCCSD(T)-F12b/VDZ-F12 on DFT geometry												
ΔE_e(min)	3.7	0.0	0.1	3.7	0	0.1	3.4	1.5	1.7			
$\Delta E_e^{\pi-\mathrm{O}}$	4.0	3.5	3.6	3.9	3.4	3.5	3.6	3.4	3.4			
$D'_e[c2\mathrm{NA_O}]$	34.6	34.4	34.5	34.6	34.4	34.5	34.4	34.5	34.5			
$D'_e[c2\mathrm{NA}_\pi]$	30.6	30.9	30.9	30.6	31.1	31.0	30.9	31.1	31.1			

Table S2 Comparison of the relative ($\Delta E_e^{\pi-\mathrm{O}}$) and absolute stabilities (D'_e) of $c2\mathrm{NA_O}$ and $c2\mathrm{NA}_\pi$ employing the B3LYP-D3$_{\mathrm{abc}}$(BJ)/def2-QZVP equilibrium geometries. All quantities are in kJ mol^{-1}.

Electronic structure	Basis	$\Delta E_e^{\pi-\mathrm{O}}$	$D'_e[c2\mathrm{NA_O}]$	$D'_e[c2\mathrm{NA}_\pi]$
PNO-LMP2	aVDZ	−6.2	51.5	57.7
PNO-LMP2	aVTZ	−2.8	44.3	47.1
PNO-LMP2-F12	VDZ-F12	−1.9	39.7	41.6
PNO-LMP2-F12	VTZ-F12	−2.2	39.0	41.2
PNO-LMP2-F12	VQZ-F12	−2.2	39.0	41.2
PNO-SCS-LMP2	aVDZ	−3.1	44.1	47.1
PNO-SCS-LMP2	aVTZ	0.5	36.9	36.4
PNO-SCS-LMP2-F12	VDZ-F12	1.4	31.9	30.5
PNO-SCS-LMP2-F12	VTZ-F12	1.1	31.1	30.1
PNO-SCS-LMP2-F12	VQZ-F12	1.1	31.2	30.1
PNO-LCCSD(T)	aVDZ	−1.8	47.6	49.4
PNO-LCCSD(T)	aVTZ	2.2	39.8	37.6
PNO-LCCSD(T)-F12b	VDZ-F12	3.5	34.5	31.0
PNO-LCCSD(T)-F12b	VTZ-F12	3.0	34.3	31.3